1-2017

Passive Scalar Transport Modeling for Hybrid RANS/LES Simulation

Zifei Yin
Iowa State University

Paul A. Durbin
Iowa State University, durbin@iastate.edu

Passive Scalar Transport Modeling for Hybrid RANS/LES Simulation

Abstract
A transport model for hybrid RANS/LES simulation of passive scalars is proposed. It invokes a dynamically computed subgrid Prandtl number. The method is based on computing test-filter fluxes. The formulation proves to be especially effective on coarse grids, as occur in DES. After testing it in a wall resolved LES, the present formulation is applied to the Adaptive DDES model of Yin et al. (Phys. Fluids 27, 025105 2015). It is validated by turbulent channel flow and turbulent boundary layer computations.

Keywords
Turbulence modeling, Hybrid RANS/LES, Detached eddy simulation, Passive scalar transport, Turbulent heat transfer, Subgrid modeling

Passive Scalar Transport Modeling for Hybrid RANS/LES Simulation

Zifei Yin
Paul A. Durbin
Iowa State University
Ames, IA 50011, USA

November 2, 2018

Abstract

A transport model for hybrid RANS/LES simulation of passive scalars is proposed. It invokes a dynamically computed subgrid Prandtl number. The method is based on computing test-filter fluxes. The formulation proves to be especially effective on coarse grids, as occur in DES. After testing it in a wall resolved LES, the present formulation is applied to the Adaptive DDES model of Yin *et al.* (2015). It is validated by turbulent channel flow and turbulent boundary layer computations.

Key words: Turbulence modeling, hybrid RANS/LES, Detached Eddy Simulation, passive scalar transport, turbulent heat transfer, subgrid modeling

1 Introduction

Hybrid RANS/LES simulation has been proposed as a means to aviod the impractical near wall grid resolution requirements of wall resolved LES, at high Reynolds numbers. Detached Eddy Simulation (DES, Spalart *et al.*, 2006; Shur *et al.*, 2008; Reddy *et al.*, 2014) is a promising hybrid formulation. Despite its origins, 'detached' eddy simulation is not longer restricted to detached shear layers. Its behavior near walls has been a subject of many studies and improvements to the methodology.

In industrial applications, heat transfer and compressibility are often encountered. That is a compelling motivation to explore methods to model scalar transport. The focus of the present article is transport of heat as a passive scalar, but it is directly relevant to compressible applications. The method is to devise a turbulent Prandtl number that adapts to the needs of either RANS or eddy-resolved simulation, as is required by DES. Adaptation is introduced by a modified version of the dynamic procedure of Large Eddy Simulation (LES), similarly to Yin *et al.* (2015).

Various turbulent Prandtl number (Pr_T) prescriptions have been proposed for RANS applications. According to Kays (1994), a value of 0.85 is generally acceptable in boundary layers.

The value of 0.9, also, is used widely. Lower values are found in free-shear layers. There also are formulas for variable turbulent Prandtl number, as a function of wall distance, or of Reynolds number (Kays *et al.*, 2012).

For LES, a *subgrid* diffusivity is needed. In isotropic turbulence, if the spectral cutoff filter lies in the inertial range, Mason & Derbyshire (1990) found a subgrid Prandtl number, $Pr_{sgs} \sim 0.4$. *A priori* tests in homogeneous shear flow (Moin *et al.*, 1991) showed that Pr_T ranged from 0.3 to 0.5, for different directions of scalar gradient.

The advantages of evaluating sub-grid model coefficients *locally and dynamically* is well recognized in the LES community. Porté-Agel (2004) proposed a dynamic formulation for heat transport. It uses a test-filtered flux to compute $C_s^2 Pr_{sgs}^{-1}$, evaluating C_s^2 via the dynamic Smagorinsky model. A scale dependent parameter, β_θ, is introduced to correct the model, if the cut-off length lies outside of the inertial range. Porté-Agel (2004) also used Lagrangian averaging to smooth the model constants.

Subgrid models based on the generalized gradient diffusion hypothesis (GGDH, Wang *et al.*, 2008) also have been proposed. Balarac *et al.* (2013) developed a regularized GGDH model, via Taylor series expansion. For reasons of stability, the regularization consisted of using only the negative definite part of the rate of strain tensor. Model constants were computed dynamically, from test-filter heat flux and small-scale similarity.

The only dynamic approach to DES is the Adaptive-DES model of Yin *et al.* (2015, see appendix). The DES portion of the present paper is an extension of that model. In Yin *et al.* (2015), the eddy viscosity is written as $\ell^2\omega$, where ω is found from the $k-\omega$ model. The length scale, ℓ is a standard DES formulation; although it differs from previous DES methods by invoking the Germano identity to compute the model constant, C_{DES}, dynamically. The assumption that C_{DES} is scale-invariant, which underlies the use of Germano's identity, breaks down on coarse grids. In such cases, a limiting function is imposed as an inferior bound on C_{DES}. In addition to evaluating the model constant locally, and dynamically, the adaptive method also reduces the size of the RANS region. Both of these elements improve predictive accuracy.

Most of the dynamic subgrid models for scalar transport have been tested only on low Reynolds number, turbulent channel flow. Here we consider high Reynolds number and boundary layer test cases, as well.

In the following, section 2 discusses the model formulation, after, first, showing how an existing heat flux model fails on a typical DES grid. Simulations of channel flow and a turbulent boundary layer are included in section 3. Some results for channel flow appear in section 2, rather than 3.1, to support the choices made in modeling.

2 Turbulent Prandtl Number

In RANS, the eddy diffusivity is commonly defined by a turbulent Prandtl number, as

$$\alpha_T = \frac{\nu_T}{Pr_T}. \tag{1}$$

The formula

$$Pr_T = \frac{1}{0.5882 + 0.2280 R_T - 0.04414 R_T^2 [1 - exp(-5.165/R_T)]}; \quad R_T \equiv \frac{k}{\omega\nu} \tag{2}$$

was proposed by Kays *et al.* (2012) for boundary layers. This asymptotes to 0.85 as $R_T \to \infty$ and to 1.7 as $R_T \to 0$. It fits the behavior of DNS data, which show that Pr_T increases right next to the wall.

In hybrid RANS/LES, the Prandtl number is required to operate in either a RANS, or a subgrid mode. The subgrid value of Pr_T can depend on grid resolution.

In some LES studies, the subgrid diffusivity was computed locally and dynamically, by a procedure based on the Germano identity (Porté-Agel, 2004). That method assumes that model constants are scale-invariant, and evaluates them as functions of discrepancies between resolved fluxes at filter and test filter scales. In extending the dynamic method to detached eddy simulation, one must be wary that the small scale spectrum may be too poorly resolved for scale invariance to be valid.

Indeed, as a preliminary, and to illustrate the needs of DES heat flux modeling, the subgrid heat flux model based on the Germano identity was tested in a DDES computation, as was the globally uniform value of $Pr_T = 0.9$. For the Germano case, Pr_T was set to be 0.9 in the RANS region and the shielding function, f_d, was used to interpolate Pr_T between RANS and eddy simulation regions.

Figure 1 shows T^+ predicted by both methods. The curve of f_d shows that the region of eddy resolved simulation lies above $y^+ = 600$ on this grid — it is a coarse grid, with $\Delta X^+ = 2\Delta Z^+ = 600$, but typical of a grid for DES. It can be seen that the simulations rise above the data correlation in the eddy resolved region.

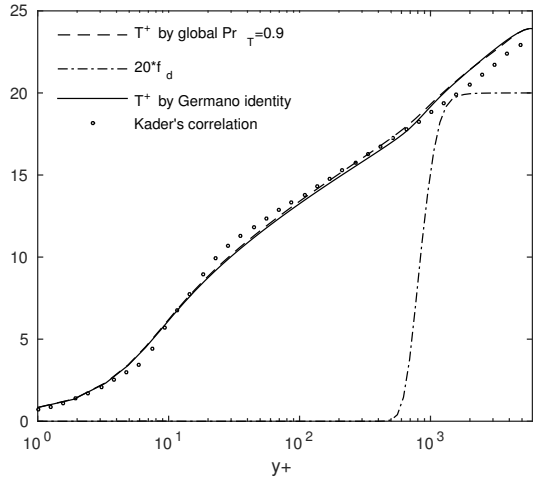

Figure 1: T^+ predicted by two methods in literature. $Re_\tau = 6,000$.

The method based on the Germano identity computes a quantity that is equivalent to C_{DES}^2/Pr_t, instead of Pr_t itself (Porté-Agel, 2004; Moin *et al.*, 1991). Time averages of the model coefficients are plotted in fig. 2. The C_{DES}^2 and C_{DES}^2/Pr_t plots, in the left pane of the

figure, show that the subgrid diffusivity is lower than subgrid viscosity in most of the eddy simulation region. The effective Pr_t, computed as the ratio of those, ranges from 0.9 to 4 in the eddy simulation region. Thus, on *coarse meshes*, the Pr_t is overestimated by this method. Temperature profiles are quite inaccurate because of this: it is not reliable, generally, for DES meshes. In the following, an alternative formulation is explored, that may be more suitable for hybrid simulations. It is, basically, to evaluate the subgrid turbulent Prandtl number directly, via test filter fluxes.

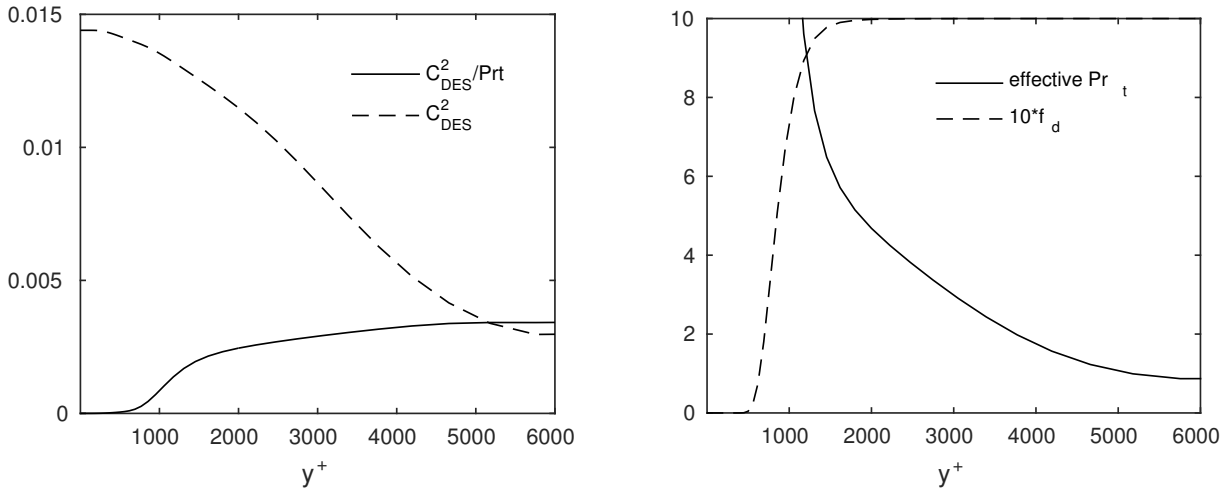

Figure 2: C^2_{DES}, C^2_{DES}/Pr_t, and Pr_t using the method based on Germano's identity in adaptive-DDES. $Re_\tau = 6,000$.

2.1 Heat Flux Model Formulation

The deviatoric stress tensor and heat flux vector on the test filter scale,

$$\begin{aligned} T_{ij} &= \widehat{u_i u_j} - \widehat{u}_i\,\widehat{u}_j - \frac{1}{3}\delta_{ij}[\widehat{u_k u_k} - \widehat{u}_k\,\widehat{u}_k] \\ F_i &= \widehat{u_i\theta} - \hat{u}_i\hat{\theta}, \end{aligned} \tag{3}$$

are computed from the resolved turbulence. They are computed locally, and dynamically during the simulation. The hat denotes explicit, test filtering (for instance, area weighted averaging over neighboring cells). The quantities being filtered are the resolved velocity and temperature fields.

To devise a formula for the Prandtl number, assume that the test filter momentum and heat fluxes are related to the rate of strain and temperature gradient by standard, eddy viscous formulae:

$$\begin{aligned} \boldsymbol{T} &= -2\hat{\nu}_{sgs}\hat{\boldsymbol{S}} \\ \boldsymbol{F} &= -\hat{\alpha}_{sgs}\cdot\boldsymbol{\nabla}\hat{\theta} \end{aligned} \tag{4}$$

$\boldsymbol{T}$ is the tensor with components T_{ij} as in eq. 3 – and similarly for $\boldsymbol{F}$. The inner products of the first of eqs. 4 with $\hat{\alpha}_{sgs}\boldsymbol{\nabla}\hat{\theta}$ and the second with $\hat{\nu}_{sgs}\hat{\boldsymbol{S}}$ give

$$\boldsymbol{T}\cdot\boldsymbol{\nabla}\hat{\theta} = 2Pr_{sgs}\hat{\boldsymbol{S}}\cdot\boldsymbol{F} \tag{5}$$

The subgrid Prandtl number is defined by $\hat{\nu}_{sgs} = Pr_{sgs}\hat{\alpha}_{sgs}$.

Pr_{sgs} can be computed from eq. 5, if it is evaluated by least square minimization:

$$Pr_{sgs} = \frac{K_i N_i}{2N_i N_i} \tag{6}$$

where $K_i = T_{ij}\partial_j\hat{\theta}$ and $N_i = \hat{S}_{ij}F_j$. Or, in tensor form,

$$Pr_{sgs} = \frac{\boldsymbol{F}\cdot\hat{\boldsymbol{S}}\cdot\boldsymbol{T}\cdot\boldsymbol{\nabla}\hat{\theta}}{2\boldsymbol{F}\cdot\hat{\boldsymbol{S}}^2\cdot\boldsymbol{F}}.$$

As described below, the Pr_{sgs} of eq. 6, additionally, was averaged spatially, to make it smoother in the eddying region.

One might object that turbulent mixing should not depend on the scalar field, contrary to eq. 6. This is called the constraint of linear superposition (Taylor, 1959). Complying with that constraint might require introducing a particle displacement tensor instead of the scalar flux tensor, and, also, abandoning the subgrid Prandtl number. The latter would not be necessary were Pr_{sgs} specified by a formula — e.g., eq. 2 satisfies the superposition constraint; the RANS Prandtl number is independent of the scalar field. In defense, one might argue that the procedure, eq. 6, uses small scale fluctuations that are insensitive to boundary and initial conditions, and hence, is in the spirit of the superposition constraint.

2.2 Test in LES and Averaging Pr_{sgs}

Since the present method is to compute a subgrid Prandtl number, it is natural, first, to test whether it is valid in wall-resolved LES, before applying it to DES.

The subgrid viscosity will be the dynamic Smagorinsky model (DSM). It defines eddy viscosity as

$$\nu_{sgs} = (C_s\Delta)^2\,|S| \tag{7}$$

Here $|S|$ is defined as $\sqrt{S_{ij}S_{ij}}$. The basic dynamic method evaluates a local model constant C_s, which is too irregular, and requires some kind of averaging to stabilize the simulation; we will apply the same averaging to Pr_{sgs}. Three possibilities can be considered: averaging over neighboring cells, averaging over homogeneous directions, and Lagrangian averaging.

The Lagrangian average proposed by Meneveau *et al.* (1996) requires the transport equations

$$\begin{aligned}\frac{Df_{lm}}{Dt} &= \frac{1}{T_L}(L_{ij}M_{ij} - f_{lm})\\ \frac{Df_{mm}}{Dt} &= \frac{1}{T_L}(M_{ij}M_{ij} - f_{mm})\end{aligned} \tag{8}$$

to be solved. L_{ij} and M_{ij} are given in eqs. A5 of the appendix, except with $|S|$ in place of ω. Then the Smagorinsky constant is evaluated as

$$C_{dyn} = max(0.0, f_{lm}/f_{mm})$$

The Lagrangian time scale is specified as

$$T_L = 1.5\Delta[f_{lm}f_{mm}]^{-1/8} \tag{9}$$

This time-scale has been criticized because it is defined by the velocity gradient, rather than a turbulence correlation (Verma & Mahesh, 2012). In DES, the integral scale of the turbulence, $T_L \sim 1/\omega$ is a suitable alternative.

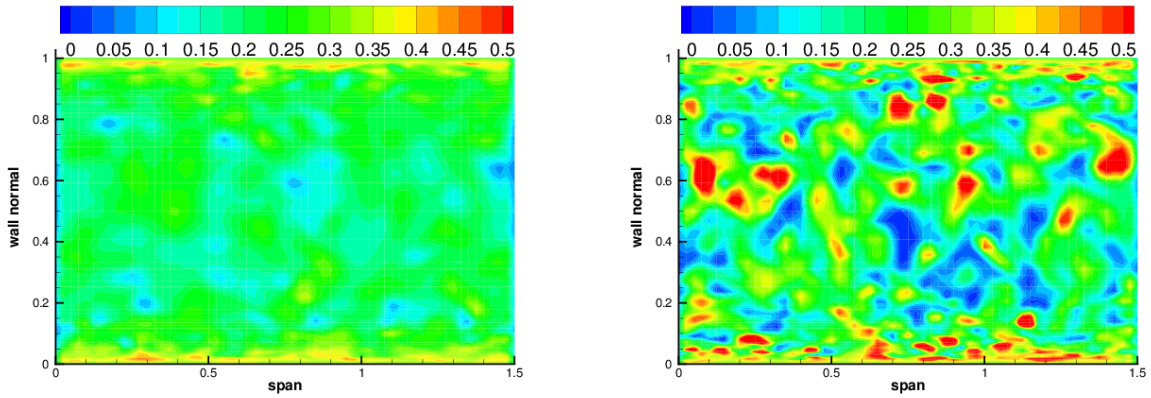

Figure 3: Lagrangian averaged, left, and local averaged contours of Pr_{sgs}.

The current dynamic procedure could locally produce large or small values for Pr_{sgs}. From a physical point of view, a subgrid Prandtl number should be on the order of 1 and not highly variable in space or time. In the literature on subgrid modeling of passive scalar transport, Lagrangian averaging has been used to smooth the eddy diffusivity (Stoll & Porté-Agel, 2006). The corresponding Lagrangian averaging for the present subgrid Prandtl number is

$$\begin{aligned} \frac{Df_{kn}}{Dt} &= \frac{1}{T_L}(K_iN_i - f_{kn}) \\ \frac{Df_{nn}}{Dt} &= \frac{1}{T_L}(N_iN_i - f_{nn}) \\ Pr_{sgs} &= max(Pr_{min}, f_{kn}/f_{nn}) \end{aligned} \tag{10}$$

where Pr_{min} is a non-zero limiting value for numerical stability. It was set to 0.01. As long as the flow is statistical stationary, the Lagrangian averaged Pr_{sgs} rarely touches that limiting value.

On the other hand, if local averaging is used, instead of a Lagrangian average, the limiting value, Pr_{min}, is invoked often. Figure 3 compares instantaneous fields with these two methods of averaging.

The Lagrangian time scale in eq. 10 is equated to T_L of eq. 9. From the point of view that turbulent transport of passive scalar is dominated by transport of momentum, the time scales for averaging subgrid heat flux and subgrid stress should be similar.

Figure 4 compares mean velocity and temperature profiles from simulations that used either local, area weighted, averages over neighboring cells, or the Lagrangian method, eqs. 8 and 10. The computational domain size is $10\delta \times 2\delta \times 3\delta$, with $100 \times 120 \times 60$ cells. The first cell height is 0.5 plus units. The grid resolution is $\Delta X^+ = 2\Delta Z^+ = 40$. The aspect ratio $\Delta X/\Delta Z = 2$ has been recommended in previous studies.

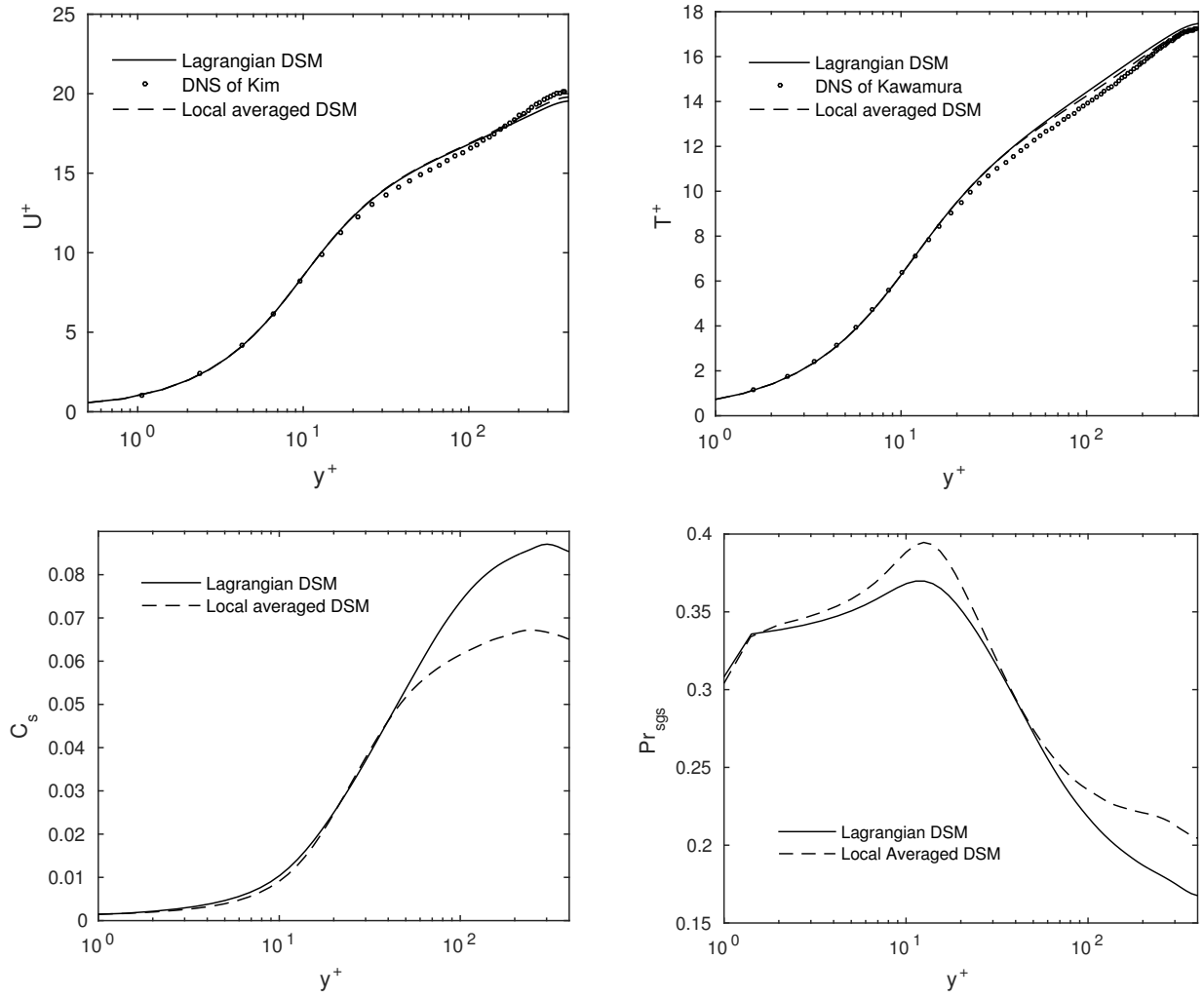

Figure 4: U^+, T^+, C_s, Pr_{sgs} for wall-resolved LES at $Re_\tau = 395$.

The velocity profile agrees with DNS data no matter which averaging process is used. It is interesting that the two different averaging processes result in different averaged value of C_s. Meneveau *et al.* (1996) compared spanwise averaging and Lagrangian averaging, which also shows some differences. The discrepancy between local averaging and Lagrangian averaging is larger than that between spanwise averaging and Lagrangian averaging. Although the C_s

distribution is different, the time averaged velocity is quite insensitive to this. As expected, C_s decreases near the wall because the resolved stress decreases.

In general, no matter what averaging process is used, the temperature profile agrees with DNS data — even a bit better than the velocity (fig. 4). Near the center of the channel, Pr_{sgs} is considerably lower than the value of 0.4 deduced in Mason & Derbyshire (1990) for homogeneous isotropic turbulence. Near the wall, the numerator and denominator of eq. 6 tend to $O(y^4)$. In fig. 4, the slope of Pr_{sgs} has an abrupt change near $y^+ = 1$; but this has no effect on the temperature profile, since turbulent mixing is negligible compared to molecular diffusion, right next to the wall,.

The present subgrid formulation for Pr_{sgs} is valid down to the solid boundary, when used in wall resolved LES. Although local averaging was found to be quite acceptable for LES, in the following sections Lagrangian averaging is used so that C_s and Pr_{sgs} have smoother fields.

When applied to DDES, the integral scale of the turbulence, $1/\omega$, is an alternative to eq. 9 for the relaxation time scale in Lagrangian averaging. For the same case at $Re_\tau = 6,000$, both equation 9 and ω are plotted in fig. 5. In the eddy simulation region, ω is nearly proportional to the Lagrangian time scale: a value of $5/\omega$ is an alternative choice to equation 9. The averaging process plays no role in the RANS region.

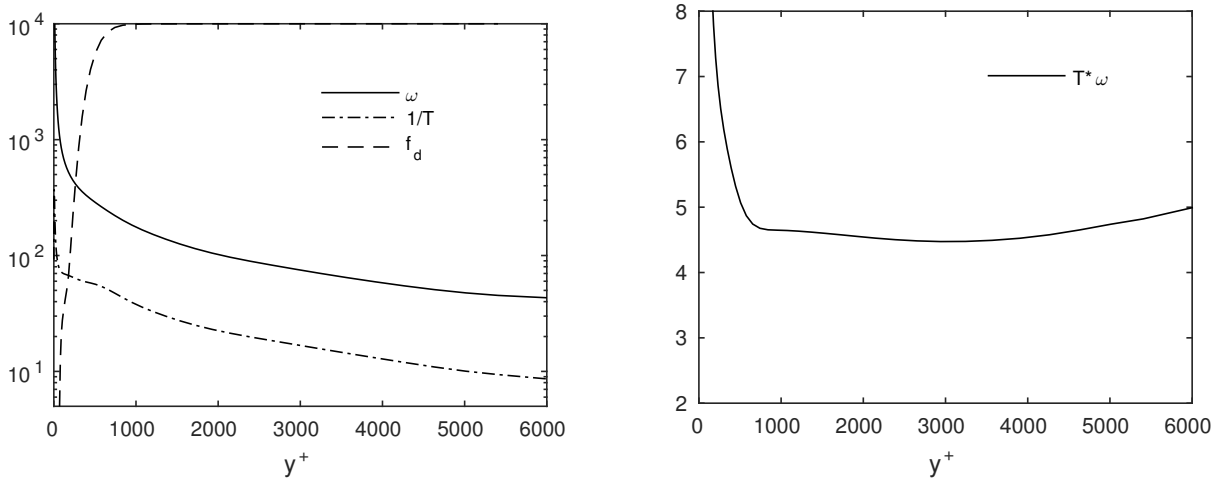

Figure 5: Lagrangian time scale and ω for adaptive-DDES at $Re_\tau = 6,000$. $f_d < 1$ is the RANS region.

2.3 Dependence on RANS Pr_T

There are different choices for the RANS value of Pr_T in the literature. Here the widely adopted value of 0.9, and the formula 2, are tested on fully developed channel flow at $Re_\tau = 6,000$ using the adaptive-DDES model. The grid and numerical set ups are the same as the case in fig. 1. Simulation results are compared with Kader (1981)'s correlation. Apparently formula 2 gives better agreement with that correlation than the widely used, 0.9 value. The right side of fig. 6 shows how the Kays & Crawford formula rises near the wall. Both models dip to the

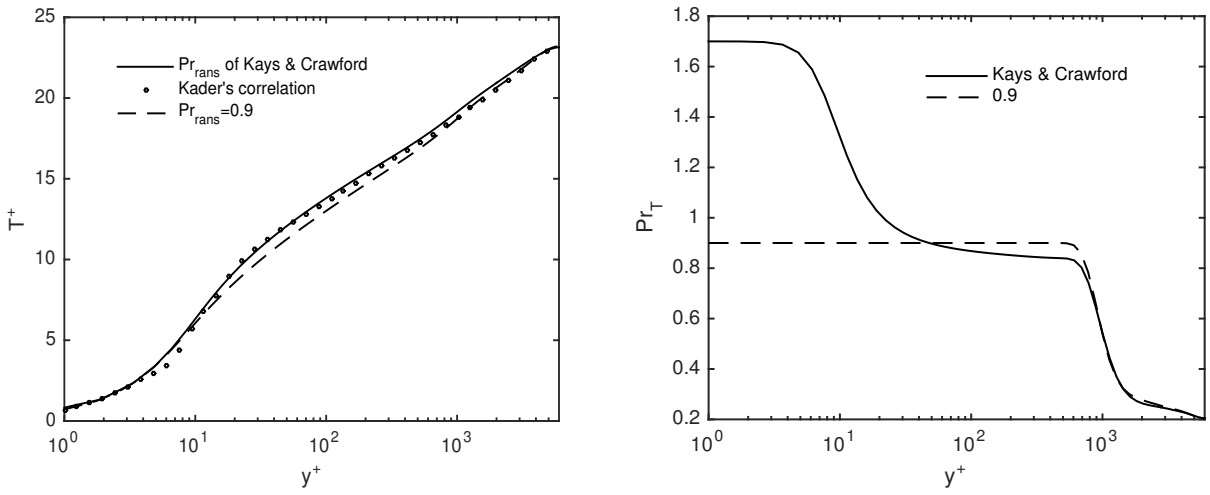

Figure 6: T^+ and Pr_T vs y^+ at $Re_\tau = 6,000$.

same level, of about $Pr_{sgs} = 0.2$, in the center of the channel, where the dynamic procedure, eq. 6, is active. The left side of fig. 6 shows the better log-layer prediction with the Kays & Crawford formula.

2.4 Interpolating Pr_T

The usual log-layer mismatch, that occurs in DDES (Spalart *et al.*, 2006), is due to depletion of the total stress when switching from RANS to eddy resolving simulation. It is alleviated in the IDDES formulation (Shur *et al.*, 2008) and the $\ell^2-\omega$ formulation (Yin *et al.*, 2015; Reddy *et al.*, 2014). In order to avoid log-layer mismatch in passive scalar transport modeling, a smooth transition from modeled stress to resolved stress is required. DDES formulations contain a shielding function f_d; it will be used to interpolate the Prandtl number. The formulation throughout the entire DDES domain is

$$\begin{aligned} \alpha_T &= \nu_T / Pr_{DES} \\ Pr_{DES} &= Pr_T + f_d \left(Pr_{sgs} - Pr_T \right) \end{aligned} \tag{11}$$

Figure 7 shows the variation of resolved heat flux and modeled heat flux in fully turbulent channel flow at $Re_\tau = 6,000$. A smooth transition from modeled stress to resolved stress is achieved. The turbulent stress distribution results in a satisfactory agreement between RANS and eddy-simulation log-layers in fig. 6.

In some situations this interpolation, eq. 11, might be problematic. f_d is a function of wall distance (eq. A1). The eddy viscosity does not have to switch to the subgrid formulation when f_d has risen from 0 to 1; it usually does, but eq. A2 allows that it might not. In that situation, the DDES model would still operate with the RANS length scale, while the Prandtl number would have switched to the subgrid formula. Even in that circumstance, the eddy viscosity is usually below the normal RANS value, so the subgrid Prandtl number might not be a bad estimate. Other ideas for interpolating Pr were not effective.

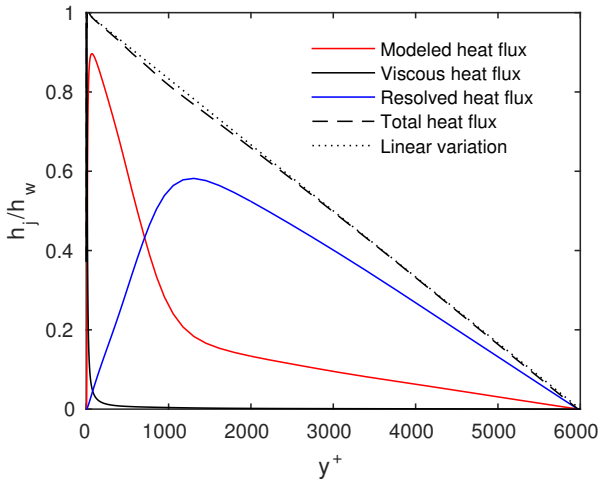

Figure 7: Modeled and Resolved Heat flux variation at $Re_\tau = 6,000$.

In summary, the present model consists of eqs. 2, 6 ,10 and 11. Eq. 2 provides the turbulent Prandtl number in the RANS region; the subgrid Prandtl number in the eddy simulation is obtained by the dynamic procedure, eq. 6, with Lagrangian averaging eq. 10. The shielding function f_d then interpolates the DES Prandtl number, per eq. 11. This model will be tested in section 3.

3 Test Cases

The proposed formulation was tested in conjunction with the adaptive, detached eddy simulation model outlined in the appendix. The open source code OpenFOAM (Jasak *et al.*, 2007) was used for all the present computer simulations. Gaussian finite volume integration, with central differencing for interpolation, was selected for spatial discretization of equations. The Sweby limiter was applied on convection terms in k and ω equations. The QUICK scheme was chosen for convection of the scalar field. Time integration was by 2^{nd} order, backward finite differences. The resulting matrix system was solved using the Pre-conditioned Bi-conjugate gradient algorithm, with the simplified, diagonal-based, incomplete-LU preconditioner. The matrix system was solved iteratively at each time step, to a specified tolerance of the residual norm.

3.1 Fully Developed Turbulent Channel Flow

Fully developed turbulent channel flow provides a basic test. The boundary conditions for inflow/outflow, and the two side boundaries are all set to periodic. The bottom and top walls are no-slip for velocity and fixed value for temperature. A uniform pressure gradient, and uniform heat source are computed from the instantaneous, averaged momentum and temperature within the channel. The sources balance the momentum and heat transferred to the walls. Thereby, the mean momentum and temperature within the whole channel are made constant

with respect to time. As the flow reaches statistical stationarity, it can be regarded as fully developed.

Results for fully developed channel flow at $Re_\tau = 6,000$ were already shown in previous sections. In order to test whether the proposed formulation is compatible with the "adaptive" character of the model outlined in the appendix, channel flow with $Re_\tau = 395$ was computed first. Comparisons with DNS data (Moser *et al.*, 1999; Kawamura *et al.*, 1999) are plotted in fig. 8. The mesh is the same as the LES simulation for $Re_\tau = 395$ in section 2.2.

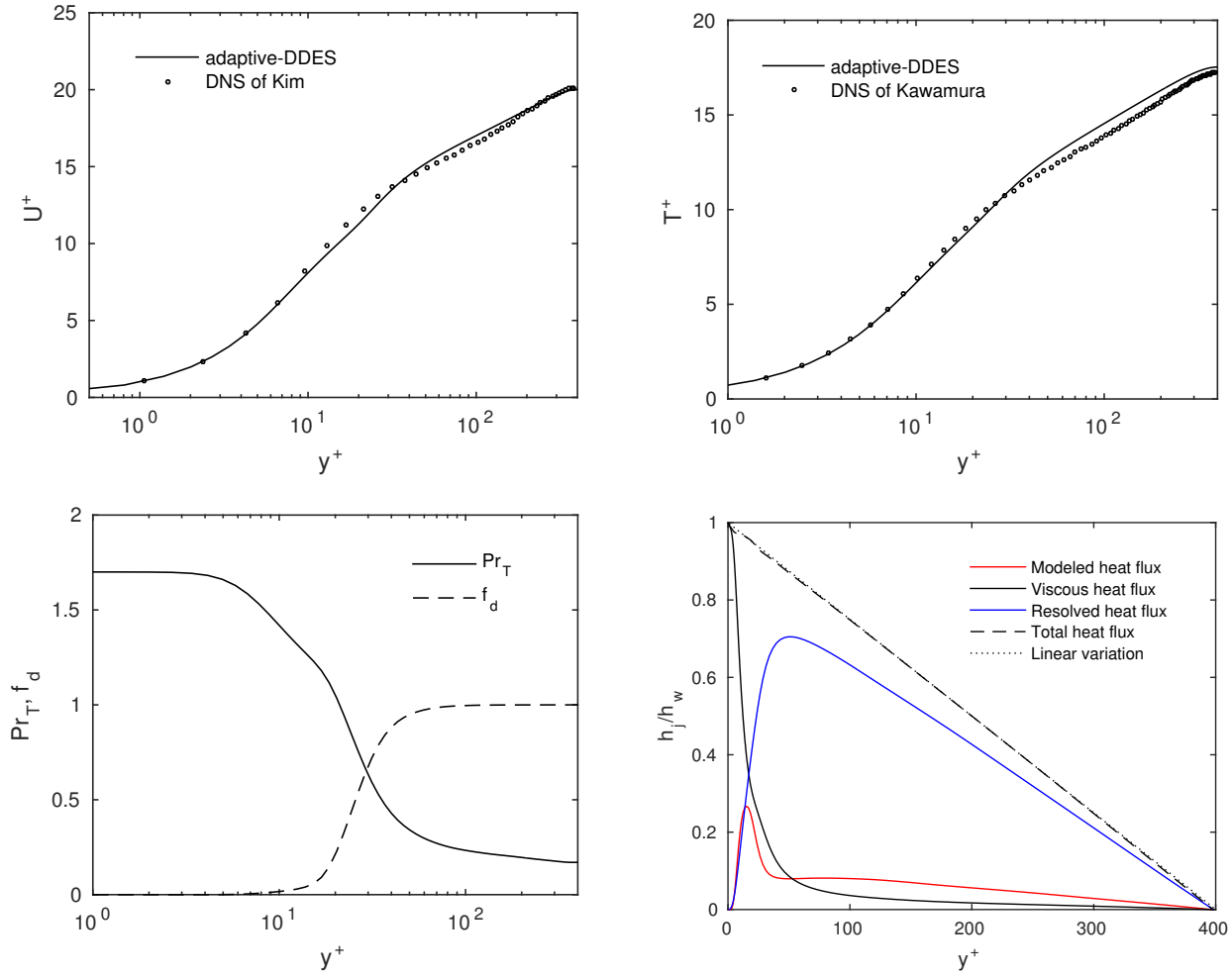

Figure 8: U^+, T^+, Pr_T, f_d and heat flux component for $Re_\tau = 395$.

Although the predicted velocity profile is not perfect, the predicted temperature agrees well with the data. The transition between RANS formula and resolved heat flux appears to be seamless, in this case. The Prandtl number distribution is interesting: there is no region where it levels out at 0.85; it is almost a continuous switch from the near-wall function ($Pr_t > 0.85$) to the subgrid Prandtl number. The plot of heat flux contributions shows that modeled heat flux is a small portion of the total everywhere. The viscous layer and buffer layer are dominated by viscous heat flux while the log-layer is dominated by resolved heat flux. Of course, that is

a consequence of this being an low Reynolds number, well resolved simulation.

Next, intermediate Reynolds number channel flow is computed with two different meshes (figure 9). The fine mesh has $100\times120\times60$ cells while the coarse mesh has half the cell numbers in both streamwise and spanwise directions. Both domain sizes are $10\delta \times 2\delta \times 3\delta$. The fine grid has a resolution of $\Delta X^+ = 2\Delta Z^+ = 225$ while the coarse grid has $\Delta X^+ = 2\Delta Z^+ = 450$. The current formulation agrees well with Kader's correlation for the mean temperature, on both grids. The small grid sensitivity shown by the temperature profile is likely to have been inherited from the velocity profile: since the scalar, subgrid diffusivity relies on the subgrid viscosity, there is an influence of momentum mixing on scalar mixing. The velocity profile is compared to a RANS computation, but at this Reynolds number the log-layer extends almost to the center of the channel, so the RANS profile, computed by $k-\omega$ model (Wilcox, 1998), is highly accurate.

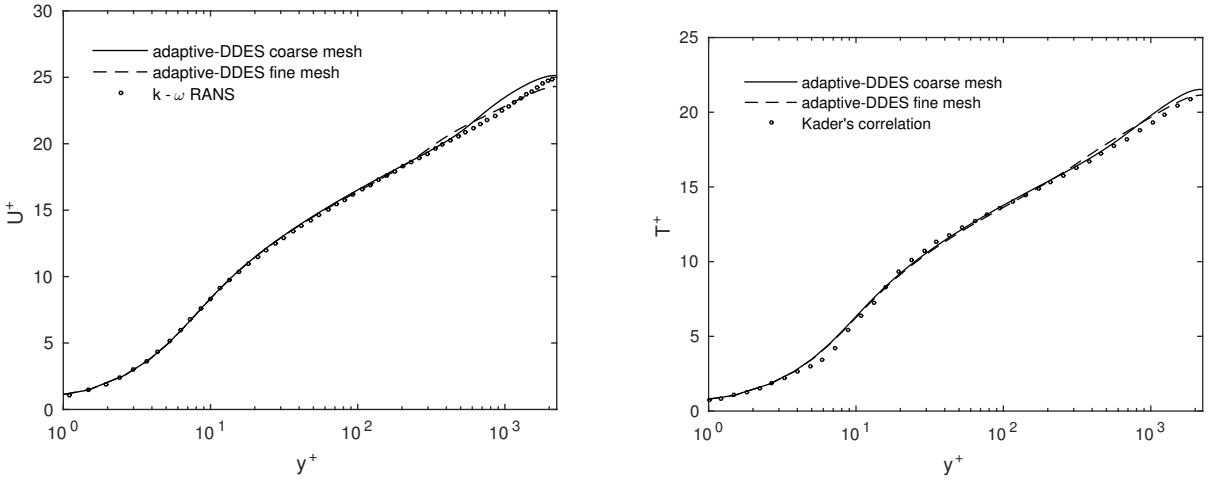

Figure 9: U^+, T^+ at $Re_\tau = 2,250$ on coarse —, and fine - - - grids.

High Reynolds number channel flow is also tested. For high Reynolds number flows, LES and DNS are too demanding to be practical, while DES can resolve eddies away from the wall with more affordable near-wall grid resolution. The case $Re_\tau = 12,000$ is shown in fig. 10. Again, the domain size is $10\delta \times 2\delta \times 3\delta$, with $100 \times 120 \times 60$ cells. The grid distribution in the wall normal direction is adjusted to have the first cell height at 0.6 plus units. In the other directions, the grid resolution is $\Delta X^+ = 2\Delta Z^+ = 1,200$. Again, the results show good agreement between prediction and correlation for passive scalar. Note that the RANS region extends to $y_+ \sim 1,000$ because the grid for this Reynolds number is coarse.

3.2 Turbulent Boundary Layer with Heat Transfer

3.2.1 Generating turbulent inflow for scalar field

Since the RANS branch of the DDES model is $k-\omega$, without a transition function, a fully turbulent boundary layer profile must be imposed as inflow. The recycling-rescaling approach of Arolla & Durbin (2014) was used to generate an unsteady, turbulent field for velocity,

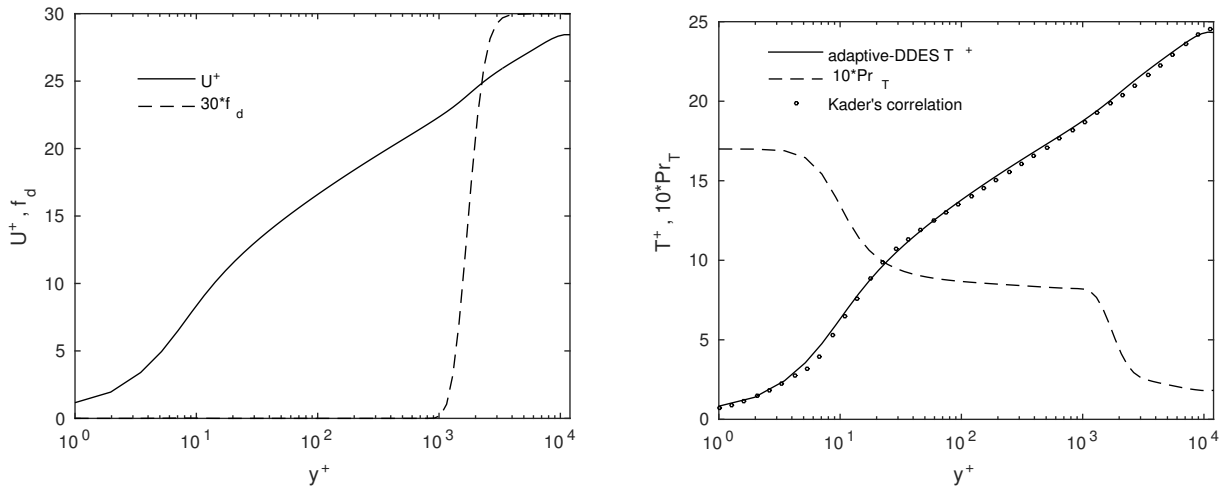

Figure 10: Left: U^+, $30\,f_d$. f_d shows the thick RANS zone. Right: T^+, $10\,Pr_T$. $Re_\tau = 12,000$.

and corresponding k and ω fields. Field variables are taken from a sample plane, located downstream of the inflow. The y coordinate of velocity, k and ω is rescaled to match a prescribed momentum thickness, then imposed at the inflow plane. However, this is not suitable for the temperature profile. In experiments and engineering applications, heat transfer may not be in equilibrium with momentum mixing.

Enthalpy is often used to describe the thermal thickness. Enthalpy thickness (δ_h) is defined as

$$\delta_h = \int_0^\infty \frac{U}{U_\infty}\left(1 - \frac{T}{T_\infty}\right) dy \tag{12}$$

Since the velocity profile is already rescaled by momentum thickness, we will not use enthalpy thickness. Instead

$$\delta_T^* = \int_0^\infty 1 - \frac{T}{T_\infty}\, dy \tag{13}$$

was used; the rescaling is

$$T(x,y,z,t)_{inlet} = T\left(x, y\frac{\delta^*_{T,sample}}{\delta^*_{T,inlet}}, z, t\right)_{sample} \tag{14}$$

This gave approximately the desired enthalpy thickness — the inlet enthalpy thickness was $0.3\% \sim 1.1\%$ lower than the targeted, experimental value. That is regarded as acceptable for present purposes.

3.2.2 Fully Developed Boundary Layer on Fixed Temperature Plate

A fully developed boundary layer was simulated and compared to data at a momentum thickness Reynolds number of $R_\Theta = 13,310$. Because the recycling method rescales y over the

entire boundary layer, rather than scaling inner and outer regions differently, the condition of strict equilibrium is broken at the inflow plane. The streamwise domain is sufficient for an equilibrium boundary layer to develop.

In the simulation the distance between the sampling and inflow planes is $9\delta_{99}$, while the entire domain is $10\delta_{99} \times 2.5\delta_{99} \times 2.5\delta_{99}$. The grid is uniformly spaced in the streamwise and spanwise directions. $\Delta X^+ = 2\Delta Z^+ = 550$ at the sampling location. The inflow momentum thickness and enthalpy thickness are adjusted to match experiment (De Graaff & Eaton, 2000) and data correlation (Kader, 1981), respectively.

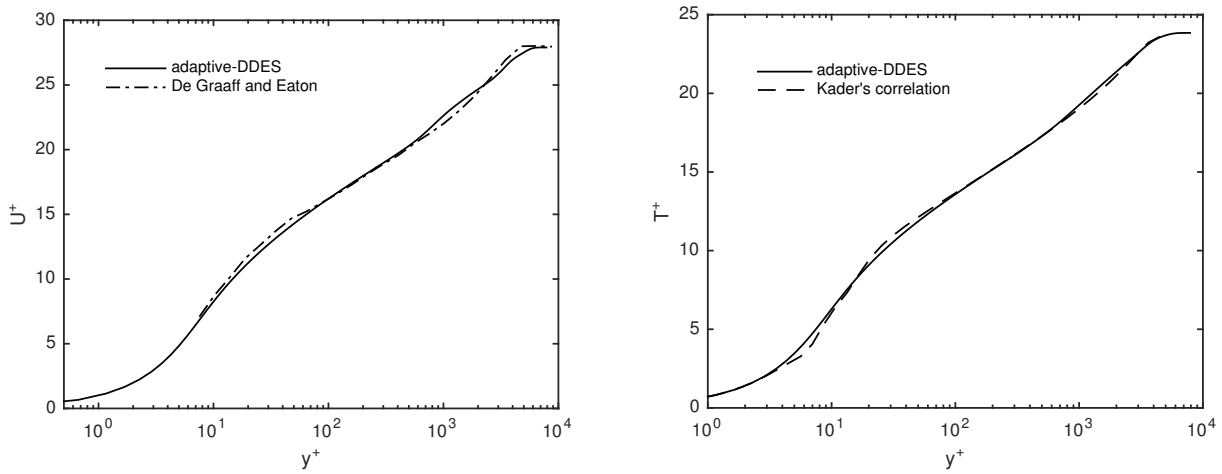

Figure 11: U^+ and T^+ versus y^+ at $Re_\Theta = 13,310$.

The velocity and temperature profiles are plotted in fig. 11. Generally, both of the computed profiles agree well with the reference data.

Figure 12 shows resolved flow structure, by the $0.05\,U_\infty$ iso-surface of instantaneous streamwise velocity fluctuation, colored with time averaged T/T_∞ and with instantaneous T'/T_∞. (Contour values on spanwise periodic planes are not properly shown by post-processing software.)

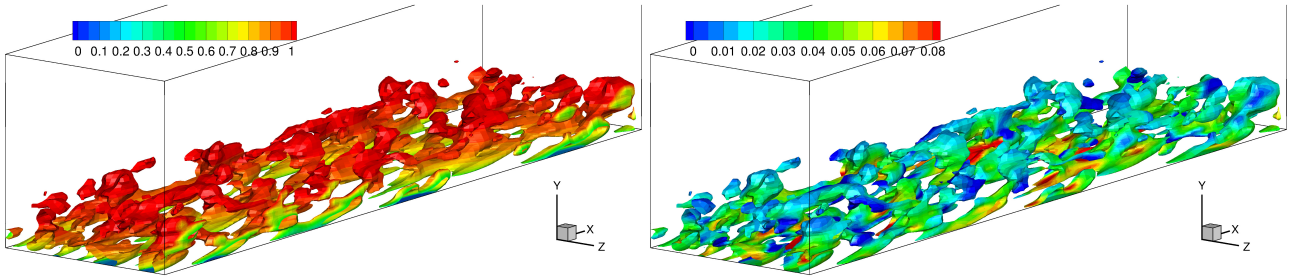

Figure 12: Iso-surface of instantaneous $u' = 5\%U_\infty$. Left: colored by time averaged T/T_∞. Right: Colored by instantaneous T'/T_∞

3.2.3 Step Heating in Zero Pressure Gradient Boundary Layer

Heat transfer in a boundary layer with a step increase in temperature was studied experimentally by Reynolds *et al.* (1958). Due to limitations in the experiment, the step is not abrupt. However, in the simulation, the temperature is increased from 0 to 1 within a distance of one cell. The step is located at $Re_\Theta = 2,280$, and the Stanton number versus Re_Θ is plotted in fig. 13.

The domain has a dimension of $55\delta_{99} \times 5\delta_{99} \times 5\delta_{99}$. This δ_{99} is measured at the step location. Because the temperature before the step is uniform, there is no need to generate unsteady inlet temperatures in this simulation. Velocity, k and ω are rescaled based on a sampling plane $15\delta_{99}$ downstream of the inlet. There are totally $220 \times 80 \times 40$ cells in the domain. The grid resolution is about $\Delta X^+ = 2\Delta Z^+ = 200$. y^+ of the first cell layer is smaller than 1. Stanton number ($St = \frac{h}{\rho U_\infty c_p}$) after the step is plotted in fig. 13.

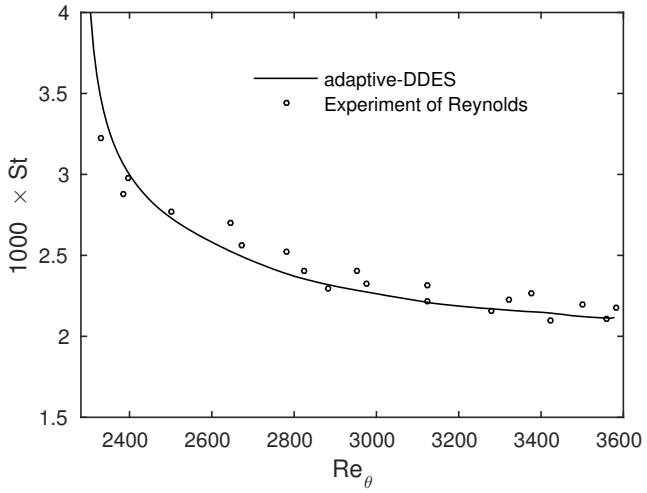

Figure 13: Stanton number versus momentum thickness Reynolds number.

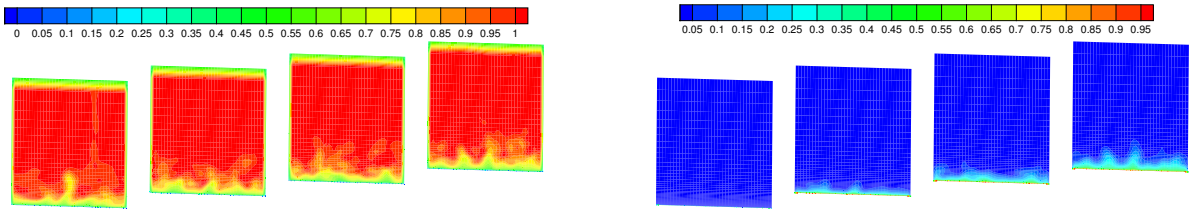

Figure 14: Instantaneous velocity U/U_∞ and temperature T/T_{wall} at various streamwise locations

The instantaneous velocity and temperature distributions are shown in fig. 14, and time averaged temperature and turbulent Prandtl number are shown in fig. 15. (Again, velocity contour values on top, zero gradient boundary planes, and side, periodic boundary planes, are not shown properly by post-processing software.) Iso-surfaces of instantaneous u' and

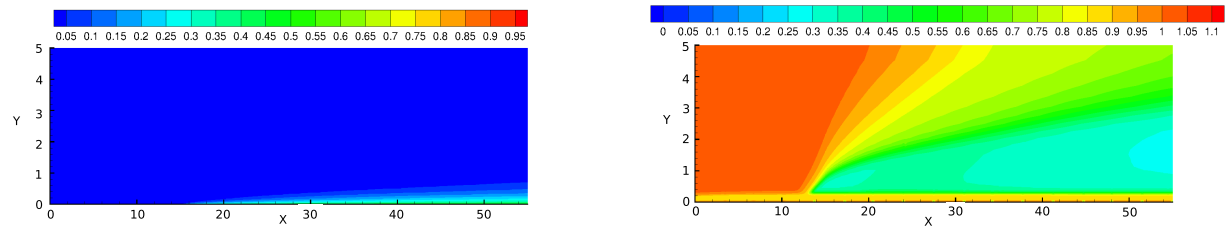

Figure 15: Time averaged T and Pr_T along streamwise and wall normal plane, coordinates normalized by δ_{99}.

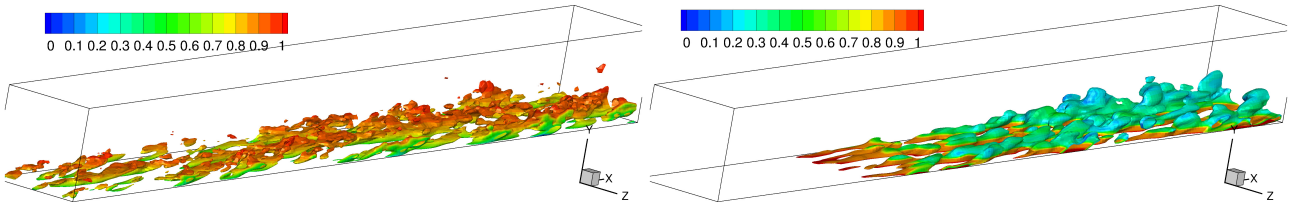

Figure 16: Left: Iso-surface of instantaneous $u' = 8\%U_\infty$, colored by time averaged U/U_∞. Right: Iso-surface of instantaneous $T' = 1\%T_{step}$, colored by instantaneous Pr_{DES}

T' are shown in figure 16. Upstream of the temperature step, the temperature is uniform. The Prandtl number is irrelevant. After the step, temperature fluctuations develop and the dynamic model adapts to the developing scalar field. Due to the uncertainty in experimental data, fig. 13 tells us the model predictions are within the correct range, but it is hard to say how large the discrepancies are.

3.3 General applicability to hybrid RANS/LES models

The dynamic procedure for computing subgrid Prandtl number can be incorporating into any hybrid RANS/LES model. The Spalart Allmaras, IDDES model (Shur *et al.*, 2008) is chosen as another example. The formulation is not changed and the interpolation between RANS Prandtl number and subgrid Prandtl number is still based on the shielding function f_d. Channel flow at $Re_\tau = 6,000$ is computed with the same mesh and numerical set ups as in section 2.3.

The velocity profile is in good agreement with the $k-\omega$ RANS prediction, as seen in fig. 17. The predicted temperature profile matches Kader's correlation reasonably well.

4 Conclusion

The present approach to passive scalar transport model is to represent it via a turbulent Prandtl number. That makes it available to various subgrid eddy viscosity formulations. The dynamic formulation was motivated by a desire to let the subgrid model adapt to the flow and to the grid. Most particularly, it aims to be an approach that is suitable on coarse grids, as can occur in detached eddy simulation. Although detached eddy simulation was the motivation, the method is equally applicable to wall resolved LES. Because it is adaptive, it is consistent

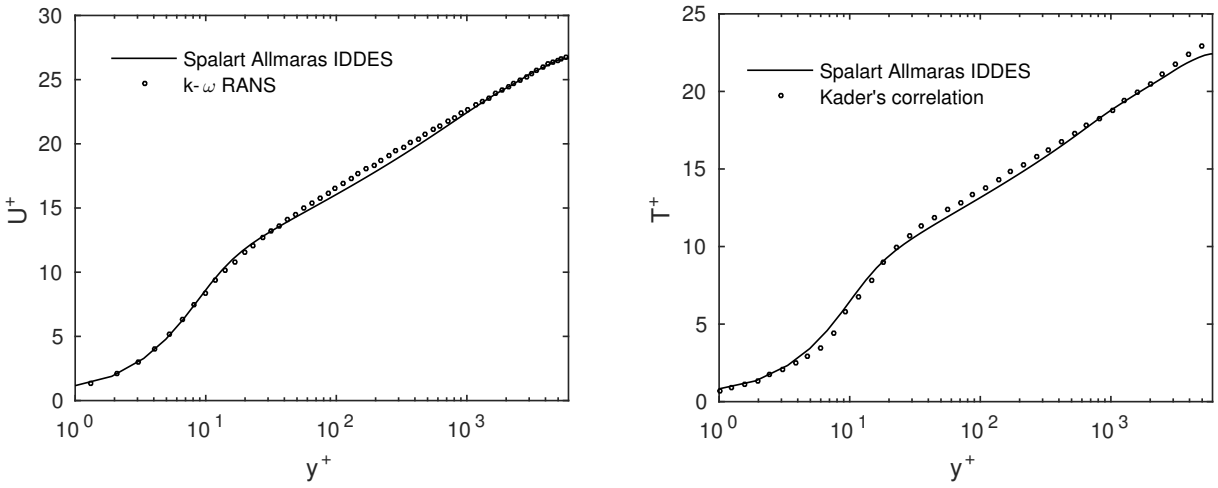

Figure 17: U^+ and T^+ vs y^+ at $Re_\tau = 6,000$.

with the dynamic Smagorinsky eddy viscosity model, and with the adaptive-DDES model. However, it was shown to work with the non-adaptive IDDES model, as well.

The accuracy of the present approach has been verified through turbulent channel flow and boundary layer simulations, with various grid resolutions and Reynolds numbers. As it is a Prandtl number formulation, it relies on a baseline subgrid eddy viscosity model. Whether it is universal for other hybrid RANS/LES methods requires testing.

5 Acknowledgements

This work was funded in part by the NASA grant NNX14AC72A, NASA Leading Edge Aeronautics grant NNX15AN98A and NSF award CBET 1507928

Appendix: Adaptive DDES model

The adaptive-DDES formulation of Yin *et al.* (2015) is summarized here. The shielding function for Delayed Detached Eddy Simulation (Spalart *et al.*, 2006) is adopted:

$$\begin{aligned} f_d &= 1 - tanh([C_{d1} r_d]^{C_{d2}}) \qquad C_{d1} = 8,\ C_{d2} = 3 \\ r_d &= \frac{k/\omega + \nu}{\kappa^2 d_w^2 \sqrt{S^2 + \Omega^2}} \end{aligned} \tag{A1}$$

where k/ω is the RANS eddy viscosity formula, ν is the molecular viscosity, κ the vonKarman constant, d_w the wall distance, S and Ω rate of strain and rate of rotation, respectively.

It is incongruous to refer to the flow as, simultaneously, being Reynolds averaged and an instantaneous realization: reference to 'RANS' and 'Eddy Simulation' regions is loose terminology. Detached eddy simulation is best described as a length scale formulation, used to

simulate realizations. The length scales and eddy viscosity are defined by

$$\left.\begin{aligned} \ell_{DDES} &= \ell_{RANS} - f_d \max(0, \ell_{RANS} - \ell_{LES}) \\ \ell_{RANS} &= \frac{\sqrt{k}}{\omega} \\ \ell_{LES} &= C_{DES}\Delta \\ \Delta &= f_d V^{1/3} + (1 - f_d) h_{max} \\ \nu_T &= \ell_{DDES}^2\, \omega \end{aligned}\right\} \tag{A2}$$

This ν_T defines the production term of the k equation in the $k-\omega$ RANS model (Wilcox, 1998), leaving all the other terms unaltered.

$$\begin{aligned} \frac{Dk}{Dt} &= 2\nu_T |S|^2 - C_\mu k\omega + \nabla \cdot [(\nu + \sigma_k(k/\omega))\nabla k] \\ \frac{D\omega}{Dt} &= 2C_{\omega 1}|S|^2 - C_{\omega 2}\omega^2 + \nabla \cdot [(\nu + \sigma_\omega(k/\omega))\nabla \omega] \end{aligned} \tag{A3}$$

The standard constants are invoked,

$$C_\mu = 0.09, \quad \sigma_k = 0.5, \quad \sigma_\omega = 0.5, \quad C_{\omega 1} = 5/9, \quad C_{\omega 2} = 3/40 \tag{A4}$$

It was shown by Yin *et al.* (2015) that an adaptive procedure can improve predictions. In their method, the dynamic procedure of LES (Lilly, 1992) is applied to the eddy viscosity (A2) to evaluate C_{DES} locally within the flow. Following that method, define the test filter stresses,

$$\begin{aligned} L_{ij} &= \widehat{u_i u_j} - \hat{u}_i \hat{u}_j \\ M_{ij} &= (\Delta^2 \widehat{\omega S_{ij}} - \hat{\Delta}^2 \hat{\omega} \hat{S}_{ij}) \end{aligned} \tag{A5}$$

These are used to determine C_{DES}; but, in order for the test filter to be valid, a significant portion of the inertial range needs to be resolved. The coarse meshes that sometimes are used in DES may not capture enough of the small scales. For this reason, a bound is placed on the computed value of C_{DES}

$$\begin{aligned} C_{dyn}^2 &= \max\left(0, 0.5 \frac{L_{ij} M_{ij}}{M_{ij} M_{ij}}\right) \\ C_{DES} &= \max(C_{lim}, C_{dyn}) \end{aligned} \tag{A6}$$

where the lower limit is determined by

$$\begin{aligned} C_{lim} &= C_{DES}^0 \left[1 - \tanh\left(\alpha \exp\left(\frac{-\beta h_{max}}{L_k}\right)\right)\right] \\ C_{DES}^0 = 0.12, \quad \alpha = 25, \quad \beta = 0.05, \quad L_k &= \left(\frac{\nu^3}{\epsilon}\right)^{1/4} \\ \epsilon &= 2(C_{DES}^0 h_{max})^2 \omega |S|^2 + C_\mu k\omega \end{aligned} \tag{A7}$$

Equation (A7) gagues the mesh resolution by comparing mesh size to the Kolmogoroff scale, L_k. If the grid is coarse, C_{DES} reverts to a default value of 0.12.

References

Arolla, Sunil K & Durbin, P. A. 2014 Generating inflow turbulence for eddy simulation of turbomachinery flows. In *52nd AIAA Aerospace Sciences Meeting, National Harbor, Maryland*.

Balarac, Guillaume, Le Sommer, Julien, Meunier, Xavier & Vollant, Antoine 2013 A dynamic regularized gradient model of the subgrid-scale scalar flux for large eddy simulations. *Physics of Fluids* **25**, 075107.

De Graaff, David B & Eaton, John K 2000 Reynolds-number scaling of the flat-plate turbulent boundary layer. *Journal of Fluid Mechanics* **422**, 319–346.

Jasak, Hrvoje, Jemcov, Aleksandar & Tukovic, Zeljko 2007 OpenFOAM: A C++ library for complex physics simulations. In *International workshop on coupled methods in numerical dynamics*, pp. 1–20.

Kader, BA 1981 Temperature and concentration profiles in fully turbulent boundary layers. *International Journal of Heat and Mass Transfer* **24**, 1541–1544.

Kawamura, Hiroshi, Abe, Hiroyuki & Matsuo, Yuichi 1999 DNS of turbulent heat transfer in channel flow with respect to Reynolds and Prandtl number effects. *International Journal of Heat and Fluid Flow* **20**, 196–207.

Kays, William M 1994 Turbulent Prandtl number, where are we? *Journal of Heat Transfer* **116**, 284–295.

Kays, William Morrow, Crawford, Michael E & Weigand, Bernhard 2012 *Convective heat and mass transfer*. Tata McGraw-Hill Education.

Lilly, Douglas K 1992 A proposed modification of the Germano subgrid-scale closure method. *Physics of Fluids A: Fluid Dynamics (1989-1993)* **4**, 633–635.

Mason, PJ & Derbyshire, SH 1990 Large-eddy simulation of the stably-stratified atmospheric boundary layer. *Boundary-layer meteorology* **53**, 117–162.

Meneveau, Charles, Lund, Thomas S & Cabot, William H 1996 A Lagrangian dynamic subgrid-scale model of turbulence. *Journal of Fluid Mechanics* **319**, 353–385.

Moin, P, Squires, K, Cabot, W & Lee, Sangsan 1991 A dynamic subgrid-scale model for compressible turbulence and scalar transport. *Physics of Fluids A: Fluid Dynamics* **3**, 2746–2757.

Moser, Robert D, Kim, John & Mansour, Nagi N 1999 Direct numerical simulation of turbulent channel flow up to $Re = 590$. *Phys. Fluids* **11**, 943–945.

Porté-Agel, Fernando 2004 A scale-dependent dynamic model for scalar transport in large-eddy simulations of the atmospheric boundary layer. *Boundary-Layer Meteorology* **112**, 81–105.

Reddy, K.R., Ryon, J.A. & Durbin, P.A. 2014 A DDES model with a smagorinsky-type eddy viscosity formulation and log-layer mismatch correction. *International Journal of Heat and Fluid Flow* **50**, 103–113.

Reynolds, William C, Kays, William Morrow & Kline, Stephen Jay 1958 Heat transfer in the turbulent incompressible boundary layer. *Tech. Rep.* 12-1-58W/PT1. NASA-Memo.

Shur, Mikhail L, Spalart, Philippe R, Strelets, Mikhail Kh & Travin, Andrey K 2008 A hybrid RANS-LES approach with delayed-DES and wall-modelled LES capabilities. *International Journal of Heat and Fluid Flow* **29**, 1638–1649.

Spalart, Philippe R, Deck, S, Shur, ML, Squires, KD, Strelets, M Kh & Travin, A 2006 A new version of detached-eddy simulation, resistant to ambiguous grid densities. *Theoretical and Computational Fluid Dynamics* **20**, 181–195.

Stoll, Rob & Porté-Agel, Fernando 2006 Dynamic subgrid-scale models for momentum and scalar fluxes in large-eddy simulations of neutrally stratified atmospheric boundary layers over heterogeneous terrain. *Water Resources Research* **42**.

Taylor, G. I. 1959 The present position in the theory of turbulent diffusion. In *Advances in Geophysics* (ed. H. E. Landsberg & J. VanMieghen), , vol. 6, pp. 101–111. Academic Press.

Verma, Aman & Mahesh, Krishnan 2012 A Lagrangian subgrid-scale model with dynamic estimation of lagrangian time scale for large eddy simulation of complex flows. *Physics of Fluids* **24**, 085101.

Wang, Bing-Chen, Yee, Eugene, Bergstrom, Donald J & Iida, Oaki 2008 New dynamic subgrid-scale heat flux models for large-eddy simulation of thermal convection based on the general gradient diffusion hypothesis. *Journal of Fluid Mechanics* **604**, 125–163.

Wilcox, David C 1998 *Turbulence modeling for CFD,* 2^{nd} *ed.* DCW industries La Canada, CA.

Yin, Z., Reddy, K.R. & Durbin, P. A. 2015 On the dynamic computation of the model constant in delayed detached eddy simulation. *Physics of Fluids* **27**, 025105.